IEEE Access
Multidisciplinary ⋮ Rapid Review ⋮ Open Access Journal

Received 3 February 2023, accepted 13 February 2023, date of publication 15 February 2023, date of current version 22 February 2023.

Digital Object Identifier 10.1109/ACCESS.2023.3245884

RESEARCH ARTICLE

High-Quality Nanocrystalline Silicon (nc-Si:H) Thin Film With Mixed-Phase and Its Application of Circulating Tumor Cell DEP Biochip

YU-MING LIN[1], (Student Member, IEEE), HUNG-WEI WU[2,5], (Senior Member, IEEE), JIA-HAO LIN[3], WEI-CHEN TIEN[3], CHENG-YUAN HUNG[3], SHOOU-JINN CHANG[1,4], (Fellow, IEEE), AND RAN LIU[5]

[1]Department of Photonics, National Cheng Kung University, Tainan 70101, Taiwan
[2]Department of Electrical Engineering, Feng Chia University, Taichung 40724, Taiwan
[3]Opto-Electronics Technology Section Energy and Agile System Department, Metal Industries Research and Development Centre, Kaohsiung 81160, Taiwan
[4]Institute of Microelectronics, Department of Electrical Engineering, Advanced Optoelectronic Technology Center, National Cheng Kung University, Tainan 70101, Taiwan
[5]Micro Nano System Center, School of Information Science and Technology, Fudan University, Shanghai 200433, China

Corresponding authors: Shoou-Jinn Chang (changsj@mail.ncku.edu.tw) and Hung-Wei Wu (hwwu@ieee.org)

This work was supported by the Taiwan's National Science and Technology Council (NSTC) under Contract MOST 111-2218-E-006-011-MBK, Contract MOST 111-2221-E-006-030-MY3, and Contract MOST 111-2823-8-035-002.

ABSTRACT This paper proposes the light-induced dielectrophoresis (DEP) biochip prepared by 40.68-MHz very high-frequency plasma-enhanced chemical vapor deposition (VHFPECVD) and post- microwave annealing treatment. The biochip can screen circulating tumor cells without using any antibodies and biomarkers. Therefore, the biochip's high efficiency and high purity are goals for effectively conducting the whole genome sequencing (WGS) analysis. The quality, uniformity, and electrical properties of the prepared silicon thin films affect the performance parameters of the biochip. High-quality nanocrystalline silicon (nc-Si:H) thin film is the core technology in the biochip. High-density nc-Si:H thin films can be well prepared using 40.68 MHz VHFPECVD and post-treatment microwave annealing. Microwave annealing improves the crystallinity and reduces the defects in the nc-Si:H thin films discovered by Fourier-transform infrared spectroscopy (FTIR). The prepared thin film with a crystallinity of 5% enhanced 38.3%, surface roughness of 10.93 nm, and a photo/dark current of 7.1×10^3 with a power density of 60mW/cm^2 was obtained. The biochip showed a recovery rate of 81.3%, purity of 78.6%, and survival rate of 91% for applying to the circulating tumor cells (CTCs).

INDEX TERMS LIDEP biochip, light-induced dielectrophoresis, nano-crystallite silicon thin film.

I. INTRODUCTION

Cancer topic has always been one topic that needs to be discussed worldwide. When cancer cells are detached from the original tumor, they will metastasize, and when metastasis occurs, they will be transmitted to other tissues through the blood [1]. Cancer cells found in the blood circulation are called CTCs. Non-invasive examination of biopsy is now a popular research method in which the metastasis and occurrence of circulating tumor cells (CTC) are related to the detection results [2], [3]. The CTCs include prostate, lung, breast, and colorectal cancers [4], [5]. CTCs as real-time liquid biopsies have recently attracted significantly [6]. During bacterial detection, it is also necessary to purify and control it at a specific concentration ratio [7]. Therefore, the discovery and monitoring of living cancer cells after isolation is also significant for cancer patients. At present, there are two standard methods for CTC separation. The first is to use the biological characteristics of cells on the label to achieve chemical identification. The other is to use the physical features of cells

The associate editor coordinating the review of this manuscript and approving it for publication was Junhua Li.

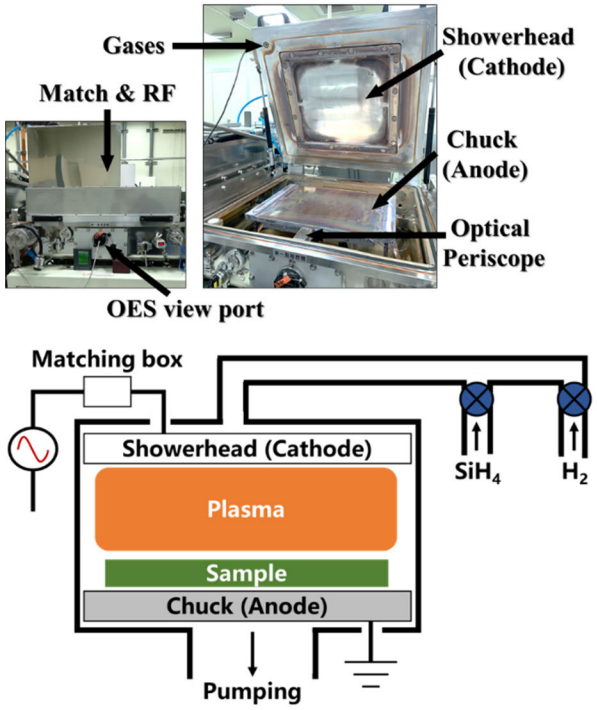

FIGURE 1. Configuration of the VHFPECVD equipment with a 40.68 MHz and plasma diagnostic tool of OES on the middle.

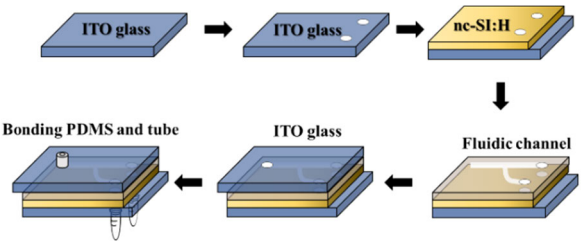

FIGURE 2. Fabrication process flow of the proposed biochip, where the main microfluidic channel with a length of 54 mm and width of 1.5 mm, and the alternative microfluidic channel with a length of 25 mm and width of 0.6 mm. The height of the microfluidic channels is defined as 50 μm for all cases.

(such as size, charge, density, etc.). The separation method used by the physical properties of dielectrophoresis (DEP) can have a high specificity [8].

DEP manipulation of particles and cells has become essential in many biotechnologies recently. Pohl first used DEP chip techniques to manipulate particles in 1951 [9]. The DEP force is a better choice for controlling cells and particles [10], [11], [12] and has the advantages of high cell activity, non-contact and high flow. However, DEP technology usually requires high design requirements and complex electrode procedures. Therefore, DEP-based extension techniques used light-induced DEP (LIDEP) to manipulate particles in 2005 [13]. LIDEP is a low-cost development technique in which optics are formed into virtual electrodes and projected onto biomedical wafers.

The LIDEP technology has been applied to manipulate different particles and cells in recent years, such as cells [7], plastic particles [14], bacteria [15], and even antibody magnetic beads [16]. However, most of them are for batch purification and separation of biological particles, and few references suggest that it is related to the properties of optoelectronic thin films. In [17], it is pointed out that the photoelectric film quality of biomedical chips is associated with the efficiency, purity, and survival rate. This study proposes exploring the optimization effect of the optoelectronic thin film properties on the biomedical wafer under different annealing methods. Some studies have pointed out that the crystalline properties of the annealed silicon film can be controlled [18], and the annealing temperature is higher than the temperature during deposition of the film, which can improve the film quality (reduce film defects) [19]. Typical LIDEP wafer photoelectric thin films are prepared from amorphous silicon films, which will produce photodegradation (S-W effect) [20] after being irradiated, thereby reducing the electrical properties of biomedical wafers. This study used the LIDEP force to cancer cells from leukocytes based on their surface area difference and electric properties [1]. The surface area of the cancer cells is always more significant than the leukocytes [2]; therefore, the amount of accumulated charges on the surface of the cells based on the optoelectronic effects depends on the surface area of the cells. When the light is projected on the nc-Si:H thin film, the nc-Si:H thin film is changed to being a low-resistivity semiconductor material, and then the cancer cells (many surface charges) and leukocytes (fewer surface charges) can be separated by moving the projected patterns to achieve the works of screening the cancer cells. Therefore, if the surface area between the two types of cells is close to approximately 5-10%, the cell screening efficiency decays significantly.

We investigated how the post-annealing process changed the properties of the photoelectric thin films and observed the differences in the properties of the photoelectric wafers. In this paper, the prepared nanocrystalline silicon thin films have the amorphous and nanocrystalline combination phase (mixed-phase). The optoelectronic characteristics of the prepared thin films are analyzed using FITR Raman, AFM, and IV measurement and discussed. It then uses the thin film repair technology (annealing process). As a result, the nanocrystalline silicon thin film's photo-dark current ratio (near 10^4) increases. The photo-dark current ratio will affect the projected pattern's electric field strength and the biomedical chip's non-projected pattern area. The crystallinity was also improved to 38.3% after annealing, and the surface roughness (RMS) was 10.93 nm. Therefore, by adjusting the photoelectric films with different power densities (40 to 70 mW/cm^2), the photoelectric films with the best photo-dark current ratio are proposed through other annealing methods. Therefore, the prepared thin film with a crystallinity of 5% enhanced 38.3%, surface roughness of 10.93 nm, and a photo/dark current of 7.1×10^3 with a power density of 60mW/cm^2 was obtained. The surface area between the

TABLE 1. The fabrication process recipe of the proposed biochip.

	Power density (mW/cm^2)	Chamber pressure (Torr)	Substrate temperature (°C)	SiH_4 (sccm)	H_2 (sccm)	Thickness (nm)
Biochip 1	40	0.6	150	110	220	750 ±3%
Biochip 2	50	0.6	150	110	220	750 ±3%
Biochip 3	60	0.6	150	110	220	750 ±3%
Biochip 4	70	0.6	150	110	220	750 ±3%

TABLE 2. Process parameters of the proposed biochip.

	Annealing method	Power density (mW/cm2)	Annealing temperature (°C)	Annealing hold time (min)	nc-Si:H Crystallinity (%)
Microwave	60	200	40	38.3	Microwave
Vacuum	60	200	40	16.7	Vacuum
Atmosphere	60	200	40	11.4	Atmosphere

two types of cells is far away, with a diameter of 20 – 60 um cancer cells and a diameter of 7 – 12 um leukocytes, which means the surface area between the two types of cells is different from about 816% to 2500%. Finally, the photoelectric films are used to prepare biomedical wafers with a purity of 78.6%, efficiency of 81.3%, and a survival rate of 91%.

II. METHODS

A. THIN FILM PREPARATION

Fig. 1 shows the VHFPECVD equipment with a 40.68 MHz and plasma diagnostic tool of OES in the middle. Including the upper and lower electrode plates and matching boxes, the electrode area is 1681 cm^2. The optical emission spectroscopy (OES) equipment is the SEMICON MC series of PLASUS, the spectrometer units of the complete UV-VIS-NIR range of 200-1000 nm, spectral resolution: 1.5 nm, time resolution: approx. 20 ms to minutes, and the Hα and SiH* characteristic lines in the plasma, at 656 and 412 nm [21], respectively, have been analyzed. Table 1 summarizes the fabrication process recipe of the proposed biochip. By tuning different power densities and different annealing methods (as shown in Table 2), after observing, the optical, electrical, and parameters are used for the biochip. The PYRO 260 Microwave System is a microwave annealing device purchased from Milestone Inc. in Italy. The vacuum annealing device is made of MIRDC, and the vacuum pressure is kept at 1×10^{-2}. Structural properties of the nc-Si:H thin films, the optimal atmosphere annealing device is DF202 DENG YNG. The FTIR spectra were recorded using an Agilent 660 spectrometer. Wavenumbers were scanned from 670 to 4000 cm^{-1} at a scan rate of 0.4 cm s^{-1}. A Renishaw Invia Raman microscope was used to study the crystallinity of the film (with a 514 nm laser). The variations of

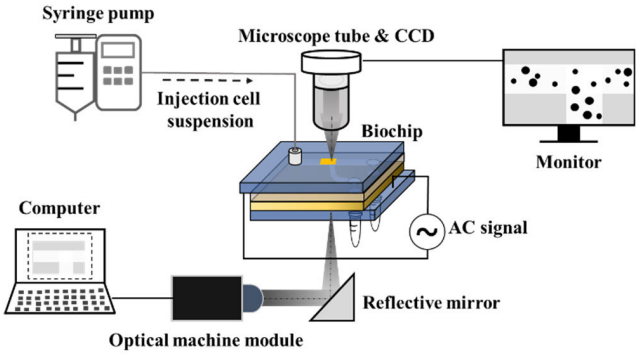

FIGURE 3. The experimental platform of the proposed biochip. The platform comprised a charge-coupled device (CCD) camera, personal computer, microscope tube, and LCD monitor.

surface morphology and root mean square (RMS) roughness as a function of before and after annealing was evaluated using an atomic force microscope (AFM, NT-MDT Solver P47 system). For the measurement of dark current (I_{dark}) and photocurrent (I_{photo}), the nc-Si:H films deposited on ITO/glass substrate were taken, and Al electrodes 2 mm apart were deposited on it by e-bean evaporation in a vacuum. The measurements were carried out at room temperature and atmospheric pressure. A voltage (0 to 3V) was applied to the Al/ITO electrodes, and an Agilent B1500 measured the current flowing through the film. A LED lamp then illuminated the film with a maximum brightness of 1500 lm.

B. BIOCHIP DESIGN

This biochip fabrication steps include step 1: the ITO glass substrate was cleaned using a standard RCA technique [22] with a 7.5 × 2.5 cm chip size. Step 2: Define two circular

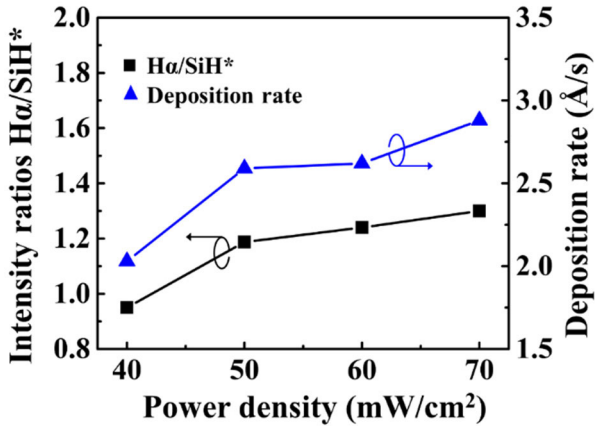

FIGURE 4. The deposition rate and the Hα/SiH∗ emission intensity of the prepared nc-Si:H thin film under different power densities of 40, 50, 60, and 70 mW/cm2 of the VHFPECVD. (The thin films thickness is 750 ± 3% nm, the process substrate temperature is 150 °C, and the chamber pressure is 0.6 Torr for all cases).

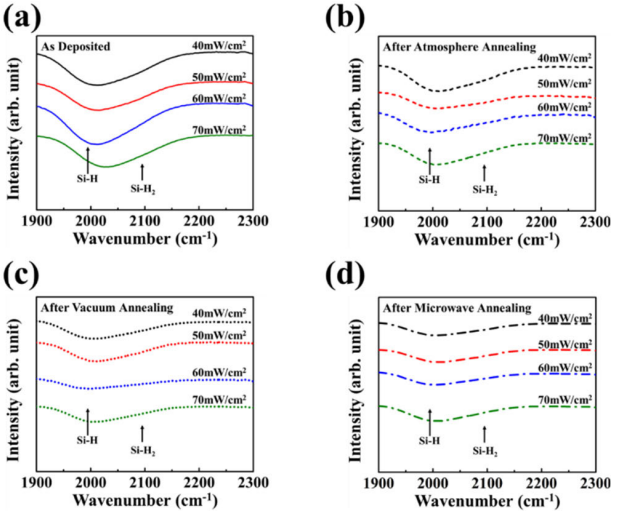

FIGURE 5. FTIR spectra of the prepared nc-Si:H thin films after post-treatment of (a) as-deposited, (b) atmosphere annealing, (c) vacuum annealing, and (d) microwave annealing as a function of the deposition power density of VHFPECVD. (The thin films thickness is 750 ± 3% nm, the process substrate temperature is 150 °C, and the chamber pressure is 0.6 Torr for all cases).

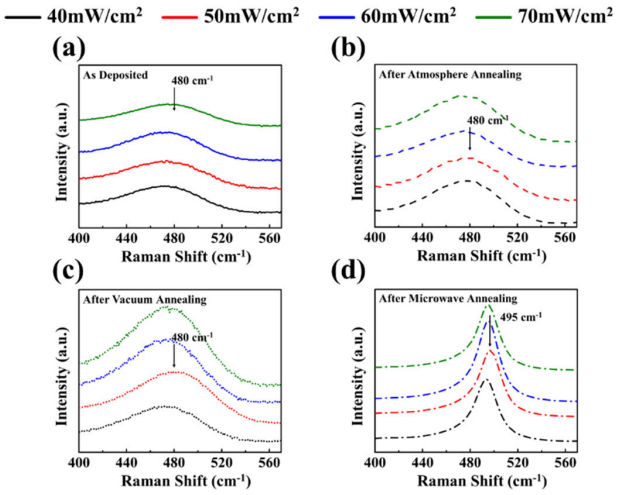

FIGURE 6. Raman spectrum of the prepared nc-Si:H thin film under different power densities of 40, 50, 60, and 70 mW/cm^2 of the VHFPECVD and having post-treatment of atmosphere annealing, vacuum annealing, and microwave annealing. (The thin films thickness is 750 ± 3% nm, the process substrate temperature is 150 °C, and the chamber pressure is 0.6 Torr for all cases).

channels in the ITO glass by laser drilling, then use the RCA second process. Step 3: VHFPECVD deposition nc-Si:H thin film with 750 ± 3% nm. Step 4: define the polydimethylsiloxane (PDMS) microfluidic channel by O2 plasma treatment. Step 5: The PDMS film was bonded on the intermediate layer between the top and bottom ITO substrate. The dimensions of the microfluidic channels are the main microfluidic channel with a length of 54 mm and width of 1.5 mm and the alternative microfluidic channel with a length of 25 mm and a width of 0.6 mm. The fabrication process flow of the proposed biochip is shown in Fig. 2.

C. CELLS PREPARATION

The preparation of the cells is defined as follows. We use the human monocytic leukemia cell line (THP-1) and human breast cancer cell line (MCF-7) in the culture media of RPMI-1640 and DMEM, respectively. The media contains 10% fetal bovine serum (FBS), 100 μg/mL streptomycin, and 100 units/mL penicillin. A cell suspension containing 0.1×10^5/ml MCF-7 cancer cells and 1.9×10^5/ml THP-1 leukocytes in 240 mM sucrose solution was prepared and followed by adding 0.25% BSA to minimize the adhesion between the cells and the inner surface of the microfluidic channel. The data were expressed as the means ± SEM. Differences were considered statistically significant when indicated by asterisks. ($* = p \leq 0.05$, $** = p \leq 0.01$, $*** = p \leq 0.001$). The experimental platform of the proposed biochip is shown in Fig. 3.

III. RESULTS AND DISCUSSIONS

A. CHARACTERISTICS OF THE PREPARED NC-SI:H THIN FILM

Fig. 4 displays the deposition rate and the Hα/SiH* emission intensity of the prepared nc-Si:H thin film with 40, 50, 60, and 70 mW/cm^2 in the VHFPECVD process. Optical emission spectra (OES) have been widely used in plasma processes for diagnostics and monitoring [23]. In this study, the OES spectra concentrating part that adopts a honeycomb structure, and the honeycomb structure has improved light collection stability and shielding dust particles. The plasma light is optically coupled via fiber into equipment. The tendency of the obtained intensity ratios Hα / SiH* is proportional to the deposition rate. This is primarily attributed to the power density increases as the dissociation and ionization of silane radicals and, thus, a resulting increase in the deposition rate [24], [25], [26]. Fig. 5 shows the Fourier transform infrared spectroscopy (FTIR) spectra of the prepared nc-Si:H thin

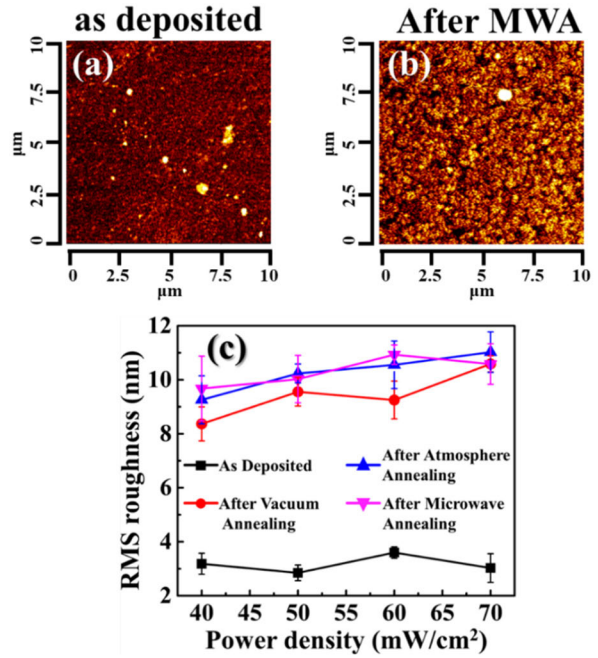

FIGURE 7. AFM images of the prepared nc-Si:H thin film under power density of 40 to 70 mW/cm^2 of the VHFPECVD and having post-treatment of atmosphere annealing, vacuum annealing, and microwave annealing (MWA). Measured and simulated 2D radiation pattern of the dual-band transparent MIMO antenna (a) at 2.1 GHz and (b) at 3.6GHz; using the frame structure (solid line) and without using the frame structure (dash line).

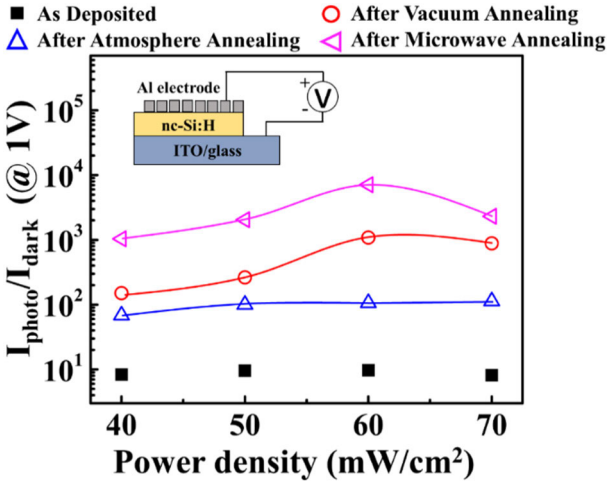

FIGURE 8. The ratio of I_{photo}/I_{dark} of the prepared nc-Si:H thin film under post-treatment of atmosphere annealing, vacuum annealing, and microwave annealing (MWA). (The thin films thickness is 750 ± 3% nm, the process substrate temperature is 150 °C and the chamber pressure is 0.6 Torr for all cases).

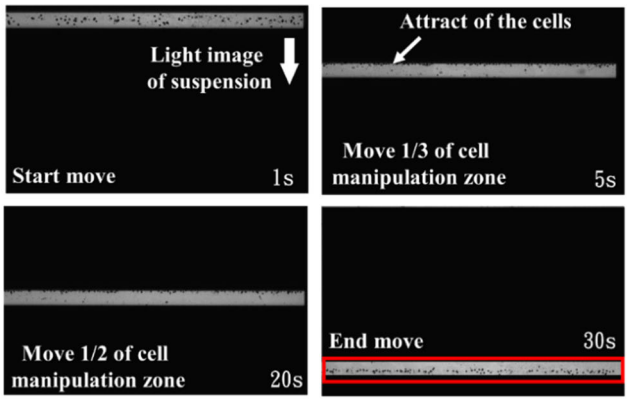

FIGURE 9. Microscopy image of the velocity of a dynamic light image for manipulating the cells. (i) the cells loaded into the microchamber of the biochip started 1 second, (ii) a moving rectangular light bar with a wide velocity range (from high to low velocity; maximum velocity: 150μm/s, set decrement: 25μm/s, minimal velocity: 20μm/s) was used to "screening" the cells within the defined cell manipulation zone from 5 to 20 seconds. (iii) The cell recovery efficiency achieved over 80% by a moving light image in 30 seconds, the maximum velocity of a dynamic light image can be defined.

films after post-treatment of as-annealing of the deposition power density of VHFPECVD. The FTIR intensity increased from Si-H to Si-H_2 when the power density was increased from 40 to 70 mW/cm^2. The increase in the Hα/SiH* ratio during the deposition process causes the increase in the hydrogen bond energies of the nc-Si:H thin film to have the peak shifts from Si–H to Si–H_2 and (Si–H_2)n bonds species. The Si–H_2 and (Si–H_2)n bonds species is about 2100 cm$^{-1,}$ stretching vibrations [27]. All the Si-H_2 intensity reduced after annealing shows the nc-Si:H thin film hydrogen content of the nc-Si:H thin film has decreased [28], and the nanocrystalline of the mixed-phase has increased [29]. Therefore, the recrystallization of nc-Si:H thin film can be achieved quickly through annealing [30]. Fig. 6 shows the Raman spectrum of the prepared nc-Si:H thin film under different power densities of 40, 50, 60, and 70 mW/cm^2 of the VHFPECVD and having post-treatment of atmosphere annealing, vacuum annealing, and microwave annealing. The cause of absorption between silicon and microwave energy is ohmic conduction loss and dielectric polarization loss. The critical factor in absorbing microwaves is the high density of dipoles (high density of defects) and proper substrate temperature [31]. After annealing post-recrystallization, all the film's Raman Shift a blue shift [32], namely the Raman peak shift to the higher wavenumber side, the crystallinity from 5% enhances to 38.3% after microwave annealing. The nc-Si:H thin film hydrogen content has decreased, as shown in Fig. 5, resulting in increased crystallinity. The degree of crystallinity also affects the nc-Si:H thin film [17]. Due to these two factors, the thin film has low defect density. It thus has high quality [33] Fig. 7 shows the AFM images of the prepared nc-Si:H thin film under a power density of 40 to 70 mW/cm^2 of the VHFPECVD and having post-treatment of atmosphere annealing, vacuum annealing, and microwave annealing (MWA). To analyze the effect of the MWA process on the surface morphology, the use of different annealing in the nc- Si:H film is observed by the formation of grains whose nanocrystalline size increases. The annealing temperature was 200 °C, the power was 400W, and the annealing was held for 40 minutes. The formation of nanocrystalline-size grains increases with the annealing time [34]. Fig. 8 shows

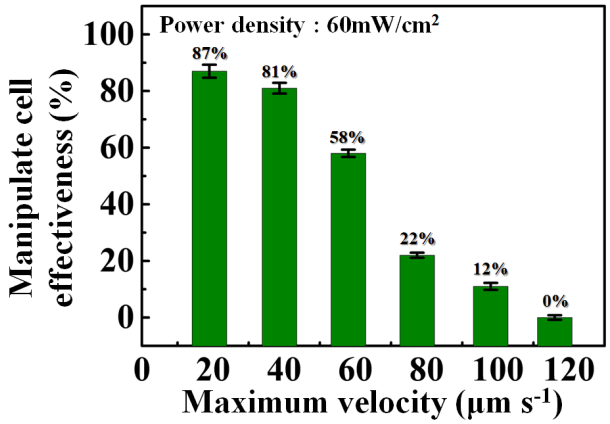

FIGURE 10. The manipulated cell efficiency of the prepared biochip 3 under the different maximum velocities after microwave annealing.

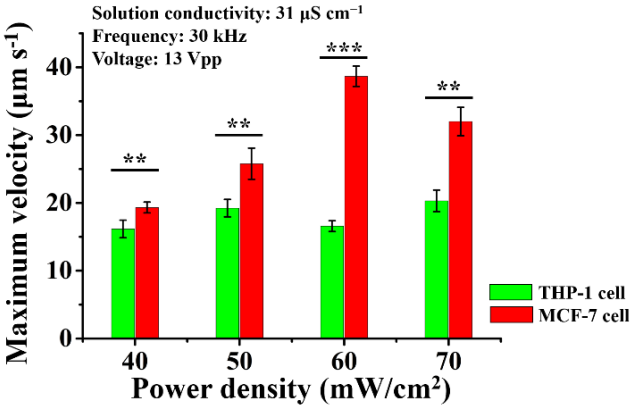

FIGURE 11. Comparison of maximum cell velocity between THP-1 cells and MCF-7 cells of the biochip.

the ratio of I_{photo}/I_{dark} of the prepared nc-Si:H thin film under post-treatment of atmosphere annealing, vacuum annealing, and microwave annealing. One of the ways to judge the electrical of the photoelectric thin film is to measure the photocurrent and dark current [35]. The I_{photo}/I_{dark} electrical properties depend on the crystallinity and grain size of the mixed-phase [36]. Appropriately increasing the crystallinity will increase the stability of the nc-Si:H thin film and reduce the occurrence of light-induced degradation [20]. The crystallinity and grain size of thin films are affected by annealing temperature [37]. Therefore, we use the metal-insulator-metal (MIM) [38] structure method to measure the nc-Si:H thin film of photo/dark current before and after annealing. As seen in the figure, In the non-annealing state, I_{photo}/I_{dark} is about 10^1, which indicates that there are still many thin film defects in the nc-Si:H thin film, although there is generated nanocrystalline.

The decrease in thin film defects observed from crystallinity, FTIR, and AFM increased 10^2-10^3 in I_{photo}/I_{dark} after microwave annealing of nc-Si:H thin film. The reduced thin film defects will also increase carrier mobility (affecting electrical characteristics) [39]. The photo/dark current depends on the crystallite size and volume fraction [40]. This can be attributed to the high defect density (dipoles) of the nc-Si:H thin film itself under high power density, the dielectric polarization loss of microwave annealing more significant (microwave energy absorption stronger) [31]. Based on the I_{photo}/I_{dark} results in Fig. 8, these measured I_{photo}/I_{dark} (i.e., after atmosphere annealing and vacuum annealing for 40, 50, 60, and 70 mW/cm^2 power density, respectively) have no greater than 10^3. The phenomena described above could indicate the difference of significance after microwave and vacuum annealing in this work. This phenomenon might lead to a more substantial bias uneven of an electric field [i.e., the ∇E^2 of Eq. (2)] for the electrically polarized cells in the light illuminated area. It could thus contribute to a higher LIDEP manipulation force than the cases after microwave annealing (i.e., The I_{photo}/I_{dark} with a power density of 60mW/cm^2 was near 10^4).

B. PERFORMANCE OF THE BIOCHIP

Fig. 9 shows the microscopy image of the velocity of a dynamic light image for manipulating the cells. The moving time of the rectangular light bar is increased. The manipulation forces that drag the cells were increased because the hydrodynamic drag force of a moving cell was used to assess the DEP manipulation force of a cell based on Stokes' law [41], [42], [43]

$$F = 6\pi r\eta v \tag{1}$$

where r, η, and v represent the radius of a cell, the viscosity of the fluid, and the terminal velocity of a cell, respectively. The moving time affects the viscosity of the liquid and cells. Impose to the AC electric voltage biochip was 13 Vpp and frequency of 30kHz, and rectangle light image (L: 2.7 mm, W: 125 μm) projected onto the biochip manipulation zone (rectangle light image moving distance was 1.1 mm, as shown in Fig. 9). After attracting the MCF-7 cells from the upper part of the manipulation zone to the 1.1mm distance, obtaining the manipulate cell efficiency ((attracted cell/ all cell) $\times$ 100%), and the manipulate cell effectiveness value exceeding 80% is defined as the maximum velocity of the biochip. To achieve screening objectives, a biochip must meet the MCF-7 cell and THP-1 cell essential difference requirements. Fig. 11 shows the comparison of maximum cell velocity between THP-1 cells and MCF-7 cells of the biochip. The experiment conditions were fixed of that THP-1 cell, and MCF-7 cell suspension was 1.5 $\times$ 10^5/ml, frequency: 30 kHz, voltage: 13 V_{pp}, solution conductivity: 31 μScm^{-1}, and calculate the cell maximum velocity of the biochip. It can be observed that biochip 3 (I_{photo}/I_{dark} of 10^3, as summarized in Table 1) is a very significant difference ($p \leq 0.001$), and the reason is that the LIDEP formula.

$$F_{DEP} = 2\pi\gamma^3\varepsilon_m \mathrm{Re}\,[f_{CM}]\,\nabla E^2 \tag{2}$$

where r, $\boldsymbol{\varepsilon_m}$, and $\boldsymbol{\nabla E^2}$ represent the radius of the microparticle, the permittivity of the medium, and the square of

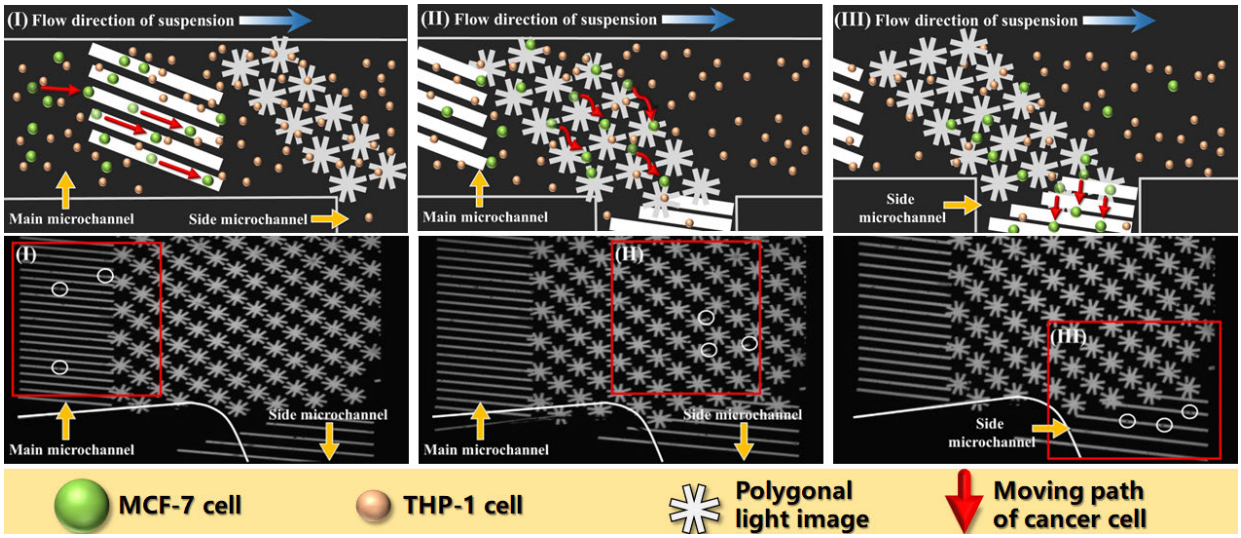

FIGURE 12. Schematic of the MCF-7 cells screening steps. (i) the cells applied DEP force by static rectangle light patterns while it flowed through the static light pattern array, and the light pattern did not influence the THP-1 cells. (ii) the MCF-7 cells were trapped, manipulated by rotating patterns, and dragged to the below microchannel. (iii) The caught MCF-7 cells were transferred into the side microchannel by a dynamic rectangle light pattern to avoid cell blockage.

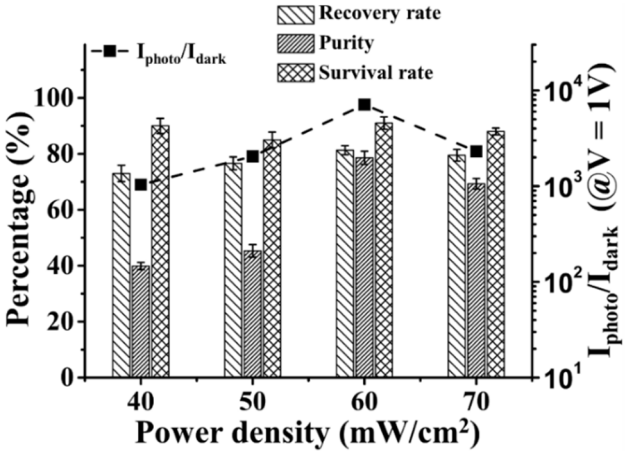

FIGURE 13. Relations of performance and I_{photo}/I_{dark} of the proposed biochips (1, 2, 3, and 4) prepared by different power densities (40, 50, 60, and 70 mW/cm^2). All experiments were repeated at least three times.

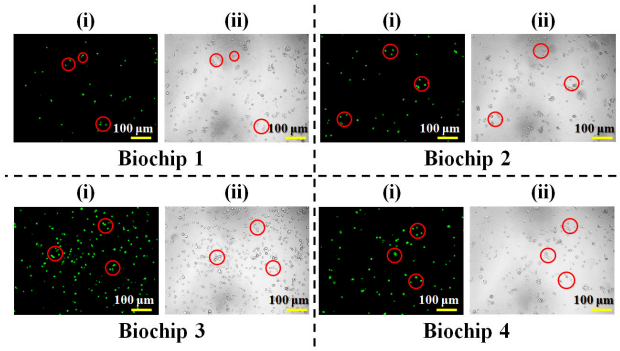

FIGURE 14. Biochips (1, 2, 3, and 4) effect of different power density (40, 50, 60, and 70 mW/cm^2) on MCF-7 cells purity analysis. To identify MCF-7 cell, the lentivirus containing pcDNA3-EGFP was used to infect MCF-7 cells. After the MCF-7 cell isolation, (i) fluorescent microscopy is to observe the MCF-7 cells (green dots), and (ii) bright-field microscopy is to observe the cell suspension with both of THP-1 cells and MCF-7 cells.

the gradient of the electrical field, respectively [44], [45]. The $\mathbf{Re}\left[f_{CM}\right]$ factor (related to the internal permittivity and conductivity). Most importantly, the I_{photo}/I_{dark} current increased closely related to $\mathbf{Re}\left[f_{CM}\right]$ factor. Fig. 12 shows the schematic of the MCF-7 cells screening process. Screening is divided into three stages: (i) the width and height were 27 um and 675 um static rectangle light pattern as a DEP force buffer in front of the main microchannel. (ii) The width and height were 0.18 mm of each dynamic light pattern and simultaneously rotated in a clockwise direction at 8.5 rpm across the main microchannel in a suspension flow zone. (iii) Avoid cell blockage above the side microchannel through the rectangle light pattern. Fig. 13 shows the relations of performance and I_{photo}/I_{dark} of the proposed biochips (1, 2, 3, and 4) prepared by different power densities of 40, 50, 60, and 70 mW/cm^2, respectively. The prepared cell suspension was loaded into the biochip at a flow rate of 1 μl min-1, followed by the MCF-7 cells isolation process. Cells suspension containing 0.5 $\times$ 10^5/ml MCF-7 cells and 2.1 $\times$ 10^5/ml THP-1 cells were prepared. Biochip 3 with a power density of 60 mW/cm^2 performs better screening the MCF-7 cells. However, these thin film defects make the two mechanisms of microwave annealing (ohmic conduction loss and dielectric polarization loss), causing the annealing effect to be more significant, and the hydrogen content of the photoelectric thin film will be reduced to produce low defect nanocrystalline. Therefore, we can conclude that the quality of the photoelectric thin film (crystallinity and I_{photo}/I_{dark}) affects biochip 1 (39.9%) and biochip 3 (78.6%); the purity

TABLE 3. Comparison of cited references and our method.

Ref.	Process method	Thin film structure	Isolation cell approaches	Cell type	I_{photo}/I_{dark}	Process time (h/ml)	Recovery rate (%)	Purity (%)	Survival rate (%)
[16]	PECVD/ Sputtering	a-Si:H	LIDEP	SW620 Cancer Cells	x	16 (2 stage)	x	86.1	x
[17]	VHFPECVD	nc-Si:H	LIDEP	Colon cancer	x	16.6	76	82	88
[43]	PECVD/ Sputtering	a-Si:H/Mo	LIDEP	Oral cancer	x	166	68	66	x
[45]	PECVD	a-Si:H	LIDEP	Liver cancer	x	~55.5	96.2	x	3
[46]	x	x	LIDEP	Saccharomyces cerevisiae	x	x	65	99.5	x
[47]	Sputtered	Cr / Au	DEP	Yeast cells	x	166	x	72.7	x
[48]	PECVD/ Sputtering	a-Si:H	LIDEP	Chondrocytes	x	166	78.3	96.4	x
This work	**VHFPECVD**	**nc-Si:H**	**LIDEP**	**Breast cancer**	**7.1×10^3**	**11~16**	**81.3**	**78.6**	**91**

(microscopic observations is shown in Fig. 14) of the biochip can be increased. Improving purity cell isolation is crucial for the subsequent gene expression and biochemistry analyses. The comparison of cited references and our method are summarized in Table 3.

IV. CONCLUSION

In this paper, the light-induced dielectrophoresis biochip prepared by 40.68-MHz very high-frequency plasma-enhanced chemical vapor deposition and having post microwave annealing treatment has been successfully proposed. The screening performance of the biochip is highly associated with the quality of the deposited nc-Si:H thin films; therefore, an appropriate deposition technique is crucial for applications in a clinical trial. Furthermore, the post-treatment of microwave annealing can effectively improve the crystallinity and reduce the defects in the nc-Si:H thin films. The prepared high-quality nc-Si:H thin film with a crystallinity of 5% enhanced to 38.3%, surface roughness of 10.93 nm, and a photo/dark current of 7.1×10^3 with a power density with a power density of 60mW/cm^2 was obtained. The biochip exhibited a recovery rate of 81.3%, purity of 78.6%, and survival rate of 91% for applying on the circulating tumor cells (CTCs). The deposition process steps and post-treatment of the prepared nc-Si:H thin films provide an effective method for a high-performance biochip. This paper offers a potential application for the antibody-free light-induced DEP biochip for circulating tumor cells screening, particularly for clinical trials.

ACKNOWLEDGMENT

The authors acknowledge the cell preparation and fundamental biochemical experiments from the Department of Biotechnology and Bioindustry Sciences, National Cheng Kung University. They would also like to acknowledge the help they received from the Metal Industries Research and Development Centre (MIRDC), Taiwan.

REFERENCES

[1] K. Pantel, R. H. Brakenhoff, and B. Brandt, "Detection, clinical relevance and specific biological properties of disseminating tumour cells," *Nature Rev. Cancer*, vol. 8, no. 5, pp. 329–340, May 2008.
[2] J.-M. Hou, M. G. Krebs, L. Lancashire, R. Sloane, A. Backen, R. K. Swain, L. J. C. Priest, A. Greystoke, C. Zhou, K. Morris, T. Ward, F. H. Blackhall, and C. Dive, "Clinical significance and molecular characteristics of circulating tumor cells and circulating tumor microemboli in patients with small-cell lung cancer," *J. Clin. Oncol.*, vol. 30, no. 5, pp. 525–532, Feb. 2012.
[3] E. Denève, S. Riethdorf, J. Ramos, D. Nocca, A. Coffy, J.-P. Daurès, T. Maudelonde, J.-M. Fabre, K. Pantel, and C. Alix-Panabières, "Capture of viable circulating tumor cells in the liver of colorectal cancer patients," *Clin. Chem.*, vol. 59, no. 9, pp. 1384–1392, Sep. 2013.
[4] C. Aggarwal, "Relationship among circulating tumor cells, CEA and overall survival in patients with metastatic colorectal cancer," *Ann. Oncol.*, vol. 24, no. 2, pp. 420–428, Oct. 2013.
[5] M. G. Krebs, R. Sloane, L. Priest, L. Lancashire, J.-M. Hou, and A. Greystoke, "Evaluation and prognostic significance of circulating tumor cells in patients with non–small-cell lung cancer," *J. Clin. Oncol.*, vol. 29, no. 12, pp. 1556–1563, Apr. 2011.
[6] K. Pantel and C. Alix-Panabières, "Real-time liquid biopsy in cancer patients: Fact or fiction?" *Cancer Res.*, vol. 73, no. 21, pp. 6384–6388, Nov. 2013.
[7] P.-Y. Chu, C.-H. Hsieh, C.-Y. Chen, and M.-H. Wu, "Improvement of background solution for optically induced dielectrophoresis-based cell manipulation in a microfluidic system," *Frontiers Bioeng. Biotechnol.*, vol. 9, Nov. 2021, Art. no. 759205.
[8] C. Alix-Panabieres and K. Pantel, "Challenges in circulating tumour cell research," *Nature Rev. Cancer*, vol. 14, no. 9, pp. 623–631, Sep. 2014.
[9] H. A. Pohl, "The motion and precipitation of suspensoids in divergent electric fields," *J. Appl. Phys.*, vol. 22, no. 7, pp. 869–871, 1951.
[10] H. S. Moon, K. Kwon, S.-L. Kim, H. Han, J. Sohn, S. Lee, and H.-I. Jung, "Continuous separation of breast cancer cells from blood samples using multi-orifice flow fractionation (MOFF) and dielectrophoresis (DEP)," *Lab a Chip*, vol. 11, no. 6, pp. 1118–1125, 2011.
[11] C. W. Shields, IV, C. D. Reyes, and G. P. López, "Microfluidic cell sorting: A review of the advances in the separation of cells from debulking to rare cell isolation," *Lab a Chip*, vol. 15, no. 5, pp. 1230–1249, 2015.
[12] H. Amini, W. Lee, and D. Di Carlo, "Inertial microfluidic physics," *Lab a Chip*, vol. 14, no. 15, pp. 2739–2761, 2014.
[13] P. Y. Chiou, A. T. Ohta, and M. C. Wu, "Massively parallel manipulation of single cells and microparticles using optical images," *Nature*, vol. 436, no. 7049, pp. 370–372, 2005.
[14] Q. Chen and Y. J. Yuan, "A review of polystyrene bead manipulation by dielectrophoresis," *RSC Adv.*, vol. 9, no. 9, pp. 4963–4981, Feb. 2019.

[15] H.-Y. Wang, C.-Y. Chen, P.-Y. Chu, Y.-X. Zhu, C.-H. Hsieh, J.-J. Lu, and M.-H. Wu, "Application of an optically induced dielectrophoresis (ODEP)-based microfluidic system for the detection and isolation of bacteria with heterogeneity of antibiotic susceptibility," *Sens. Actuators B, Chem.*, vol. 307, Mar. 2020, Art. no. 127540.

[16] P.-Y. Chu, C.-H. Hsieh, and M.-H. Wu, "The combination of immunomagnetic bead-based cell isolation and optically induced dielectrophoresis (ODEP)-based microfluidic device for the negative selection-based isolation of circulating tumor cells (CTCs)," *Frontiers Bioeng. Biotechnol.*, vol. 8, p. 921, Aug. 2020.

[17] J.-H. Lin, H.-W. Wu, W.-C. Tien, C.-Y. Hung, H.-Y. Lai, and S.-K. Liu, "High-efficiency light-induced circulating tumor cells screening biochip prepared by 40.68-MHz VHFPECVD," *IEEE Sensors J.*, vol. 20, no. 16, pp. 8938–8946, Aug. 2020.

[18] F. Yang, X. Li, Z. Ren, G. Xu, Y. Liu, G. Shen, and G. Han, "The nc-Si films with controlled crystal structure and electrical conductivity via the recrystallization approach," *J. Non-Crystalline Solids*, vol. 359, pp. 40–45, Jan. 2013.

[19] C. H. Lee, D. J. Grant, A. Sazonov, and A. Nathan, "Postdeposition thermal annealing and material stability of 75 °C hydrogenated nanocrystalline silicon plasma-enhanced chemical vapor deposition films," *J. Appl. Phys.*, vol. 98, no. 3, Aug. 2005, Art. no. 034305.

[20] X. Y. Han, Y. Wang, J. M. Xue, S. W. Zhao, Y. X. Li, and X. H. Geng, "Stability of microcrystalline silicon materials under light soaking," *Mater. Sci. Semicond. Process.*, vol. 9, nos. 1–3, pp. 300–303, Feb./Jun. 2006.

[21] G. Hou, J. Xue, Y. Yuan, J. Sun, Y. Zhao, and X. Geng, "A fast method to diagnose phase transition from amorphous to microcrystalline silicon," *Sci. China G, Phys., Mech. Astron.*, vol. 50, no. 6, pp. 731–736, Dec. 2007.

[22] X. L. Liang, B. A. Sperling, I. Calizo, G. Cheng, and C. A. Hacker, "Toward clean and crackless transfer of graphene," *ACS Nano*, vol. 5, no. 11, pp. 9144–9153, Nov. 2011.

[23] H. H. Yue, S. J. Qin, R. J. Markle, C. Nauert, and M. Gatto, "Fault detection of plasma etchers using optical emission spectra," *IEEE Trans. Semicond. Manuf.*, vol. 13, no. 3, pp. 374–385, Aug. 2000.

[24] S. Lebib and P. Roca i Cabarrocas, "Effects of ion energy on the crystal size and hydrogen bonding in plasma-deposited nanocrystalline silicon thin films," *J. Appl. Phys.*, vol. 97, no. 10, May 2005, Art. no. 104334.

[25] K. Bhattacharya and D. Das, "Nanocrystalline silicon films prepared from silane plasma in RF-PECVD, using helium dilution without hydrogen: Structural and optical characterization," *Nanotechnology*, vol. 18, no. 41, Oct. 2007, Art. no. 415704.

[26] L. Guo, M. Kondo, M. Fukawa, K. Saitoh, and A. Matsuda, "High rate deposition of microcrystalline silicon using conventional plasma-enhanced chemical vapor deposition," *Jpn. J. Appl. Phys.*, vol. 37, no. 10A, p. L1116, Oct. 1998.

[27] D. V. Tsu, G. Lucovsky, and B. N. Davidson, "Effects of the nearest neighbors and the alloy matrix on SiH stretching vibrations in the amorphous SiO_r:H ($0 < r < 2$) alloy system," *Phys. Rev. B, Condens. Matter*, vol. 40, no. 3, pp. 1795–1805, Jul. 1989.

[28] U. Kroll, J. Meier, A. Shah, S. Mikhailov, and J. Weber, "Hydrogen in amorphous and microcrystalline silicon films prepared by hydrogen dilution," *J. Appl. Phys.*, vol. 80, no. 9, pp. 4971–4975, Nov. 1996.

[29] J.-H. Shim and N.-H. Cho, "Structural and chemical features of silicon nanocrystallites in nanocrystalline hydrogenated silicon thin films," *Glass Phys. Chem.*, vol. 31, no. 4, pp. 525–529, Jul. 2005.

[30] M. Zacharias, L. Tsybeskov, K. D. Hirschman, P. M. Fauchet, J. Bläsing, P. Kohlert, and P. Veit, "Nanocrystalline silicon superlattices: Fabrication and characterization," *J. Non-Crystalline Solids*, vols. 227–230, pp. 1132–1136, May 1998.

[31] C. Fu, Y. Wang, P. Xu, L. Yue, F. Sun, D. W. Zhang, S.-L. Zhang, J. Luo, C. Zhao, and D. Wu, "Understanding the microwave annealing of silicon," *AIP Adv.*, vol. 7, no. 3, Mar. 2017, Art. no. 035214.

[32] C. Y. Xu, P. X. Zhang, and L. Yan, "Blue shift of Raman peak from coated TiO_2 nanoparticles," *J. Raman Spectrosc.*, vol. 32, no. 10, pp. 862–865, Oct. 2001.

[33] Y. Wang, H. Liu, and W. Shen, "A convenient and effective method to deposit low-defect-density nc-Si: H thin film by PECVD," *Nanoscale Res. Lett.*, vol. 13, no. 1, pp. 1–9, Aug. 2018.

[34] M. Rojas-Lopez, A. Orduña-Diaz, R. Delgado-Macuil, V. L. Gayou, and R. E. Pérez-Blanco, "Morphological transformation and kinetic analysis in the aluminum-mediated a-Si:H crystallization," *J. Non-Crystalline Solids*, vol. 352, no. 3, pp. 281–284, Mar. 2006.

[35] N. E. Koksal, M. Sbeta, and A. Yildiz, "GZO/Si photodiodes exhibiting high photocurrent-to-dark-current ratio," *IEEE Trans. Electron Devices*, vol. 66, no. 5, pp. 2238–2242, May 2019.

[36] S. Juneja, S. Sudhakar, J. Gope, and S. Kumar, "Mixed phase silicon thin films grown at high rate using 60 MHz assisted VHF-PECVD technique," *Mater. Sci. Semicond. Process.*, vol. 40, pp. 11–19, Dec. 2015.

[37] N. M. Ahmed, F. A. Sabah, H. I. Abdulgafour, A. Alsadig, A. Sulieman, and M. Alkhoaryef, "The effect of post annealing temperature on grain size of indium-tin-oxide for optical and electrical properties improvement," *Results Phys.*, vol. 13, Jun. 2019, Art. no. 102159.

[38] S. A. Dereshgi and A. K. Okyay, "Large area compatible broadband superabsorber surfaces in the VIS-NIR spectrum utilizing metal-insulator-metal stack and plasmonic nanoparticles," *Opt. Exp.*, vol. 24, no. 16, pp. 17644–17653, Aug. 2016.

[39] C.-H. Lee, A. Sazonov, and A. Nathan, "High-mobility nanocrystalline silicon thin-film transistors fabricated by plasma-enhanced chemical vapor deposition," *Appl. Phys. Lett.*, vol. 86, no. 22, May 2005, Art. no. 222106.

[40] T. Saitoh, T. Shimada, M. Migitaka, and Y. Tarui, "Preparation and properties of microcrystalline silicon films using photochemical vapor deposition," *J. Non-Crystalline Solids*, vols. 59–60, pp. 715–718, Dec. 1983.

[41] T. K. Chiu, WP Chou, S. B. Huang, H. M. Wang, and Y. C. Lin, "Application of optically-induced-dielectrophoresis in microfluidic system for purification of circulating tumour cells for gene expression analysis—Cancer cell line model," *Sci. Rep.*, vol. 6, p. 32851, Sep. 2016.

[42] S. B. Huang, M. H. Wu, Y. H. Lin, C. H. Hsieh, and C. L. Yang, "High-purity and label-free isolation of circulating tumor cells (CTCs) in a microfluidic platform by using optically-induced-dielectrophoretic (ODEP) force," *Lab a Chip*, vol. 13, no. 7, pp. 1371–1383, 2013.

[43] S. B. Huang, J. Chen, J. B. Wang, C. L. Yang, and M. H. Wu, "A new optically-induced dielectrophoretic (ODEP) force-based scheme for effective cell sorting," *Int. J. Electrochem. Sci.*, vol. 7, no. 12, pp. 12656–12667, Dec. 2012.

[44] H. A. Pohl, *Dielectrophoresis: The Behavior of Neutral Matter in Nonuniform Electric Fields*. Cambridge, U.K.: Cambridge Univ. Press, 1978.

[45] J. K. Valley, A. Jamshidi, A. T. Ohta, H. Y. Hsu, and M. C. Wu, "Operational regimes and physics present in optoelectronic tweezers," *J. Microelectromech. Syst.*, vol. 17, no. 2, pp. 342–350, Apr. 2008.

[46] M. Du, G. Li, Z. Wang, Y. Ge, and F. Liu, "Rapid isolation method of Saccharomyces cerevisiae based on optically induced dielectrophoresis technique for fungal infection diagnosis," *Appl. Opt.*, vol. 60, no. 8, pp. 2150–2157, Mar. 2021.

[47] I. Doh and Y. H. Cho, "A continuous cell separation chip using hydrodynamic dielectrophoresis (DEP) process," *Sens. Actuators A, Phys.*, vol. 121, no. 1, pp. 59–65, 2005.

[48] H. Song-Bin, L. Shing-Lun, L. Jian-Ting, and W. Min-Hsien, "Label-free live and dead cell separation method using a high-efficiency optically-induced dielectrophoretic (ODEP) force-based microfluidic platform," *Int. J. Autom. Smart Technol.*, vol. 4, no. 2, pp. 83–91, Jun. 2014.